Journal of Alloys and Compounds 505 (2010) 315–318

Contents lists available at ScienceDirect

Journal of Alloys and Compounds

journal homepage: www.elsevier.com/locate/jallcom

Mechanical and magnetic properties of $(Fe_{72}Mo_4B_{24})_{100-x}Tb_x$ (x = 4, 5, 6, 7 at.%) bulk glassy alloys

Hong Jian, Wei Luo, Shan Tao, Mi Yan*

State Key Laboratory of Silicon Materials, Department of Materials Science and Engineering, Zhejiang University, Hangzhou 310027, China

ARTICLE INFO

Article history:
Received 22 January 2010
Received in revised form 7 June 2010
Accepted 10 June 2010
Available online 17 June 2010

PACS:
75.50.Bb, 75.60.Ej, 64.70.Pf

Keywords:
Fe-based amorphous alloy
Bulk metallic glass
Glass forming ability
Mechanical property
Magnetic property

ABSTRACT

$(Fe_{72}Mo_4B_{24})_{100-x}Tb_x$ (x = 4, 5, 6, 7 at.%) bulk glassy alloys with diameter of 2 mm were prepared by copper mold casting. The influence of Tb content on glass forming ability was investigated. There is partial crystallization in the alloy when x = 4, while fully amorphous alloys with no detectable crystallization are obtained for x = 5, 6, 7, respectively. DSC curves of the amorphous alloys indicate that this system exhibits a high glass transition temperature (T_g = 848–927 K) and a wide supercooled liquid region up to 104 K. The best glass forming ability is obtained for x = 5. These bulk metallic glasses exhibit good mechanical properties, with the compressive strength up to 3163 MPa, and H_v up to 1149. In addition, the alloys exhibit relatively good soft magnetic properties, with M_s up to 69.205 emu/g and H_c as low as 4 Oe.

1. Introduction

Since Fe-based bulk metallic glass (BMG) was firstly synthesized in Fe–Al–Ga–P–C–B system by Inoue et al. [1], a lot of researches have been done on Fe-based bulk metallic glasses. Fe-based BMGs, with high fracture strength and hardness, good corrosion resistance, excellent soft magnetic properties as well as low cost, have great potential both as functional and structural materials. Three empirical rules for the development of amorphous alloys were proposed by Inoue [2]: (1) multicomponent alloy systems consisting of more than three elements; (2) significant difference in atomic size ratio above 12% among the main three elements; (3) negative heats of mixing among their elements. Upon these empirical rules, various BMG systems have been developed, such as Fe–(Al, Ga)–(P, C, B, Si) [3,4], Fe–(Co, Ni)–(Zr, Nb, Ta, Mo, W, Hf)–B [5–13], Fe–(Co, Ni)–M–Si–B (M = Nb, Zr) [14–17]. The effect of rare earth addition on glass forming ability has been investigated in (Fe, Co)–La–TM–B (La = lanthanide metal, TM = transition metal) systems [18–21]. La addition is proved to be able to improve the glass forming ability in these alloy systems. The local ordering structure of $Fe_{67}Co_{10}La_3B_{20}$ (La = Sm, Tb, Dy) amorphous alloys has been studied by Imafuku et al. [19]. It is recognized that La atom plays an important role in the formation of the dense random packing structure of (Fe, Co)–B in these alloys. However, no BMGs were prepared in these alloys. In order to enhance glass forming ability in Fe–Nb–B ternary system, Song et al. investigated the effect of Y addition, and successfully prepared BMGs with a diameter up to 2 mm [22]. Subsequently, other BMGs with good glass forming ability were prepared with Y addition [23–26]. However, relatively few works have been done on the effect of other La element addition on the glass forming ability. Considering similarity in La elements, other rare earth elements might also benefit the formation of BMG in Fe-based alloy system. Previous investigations have also suggested that the incorporation of thermally stable refractory elements can stabilize the amorphous structure of Fe-based BMGs [14,23,27,28]. As Mo is also a refractory element like Nb, $Fe_{72}Mo_4B_{24}$ was chosen as the precursor in this work. This paper intends to present the composition dependence of thermal stability of the supercooled liquid region, mechanical and magnetic properties in $(Fe_{72}Mo_4B_{24})_{100-x}Tb_x$ (x = 4, 5, 6, 7 at.%).

2. Experimental procedures

Multicomponent $Fe_{72}Mo_4B_{24}$ ingot was prepared by induction melting pure Fe, Mo and pre-alloyed FeB (B content 21.36 wt.%) in an argon atmosphere. The ingot was crushed into small pieces and mixed with pure Tb metal quantitatively in accord with the composition of $(Fe_{72}Mo_4B_{24})_{100-x}Tb_x$ (x = 4, 5, 6, 7 at.%). The mixture was remelted and cast into a copper mold in argon atmosphere to obtain rods with diameter of 2 mm. Structure of the as-cast rods was examined by X-ray diffraction (XRD) with Cu Kα radiation. High-resolution transmission electron microscope (HRTEM)

* Corresponding author. Tel.: +86 571 87952730; fax: +86 571 87952730.
E-mail address: mse_yanmi@zju.edu.cn (M. Yan).

0925-8388/$ – see front matter © 2010 Elsevier B.V. All rights reserved.
doi:10.1016/j.jallcom.2010.06.061

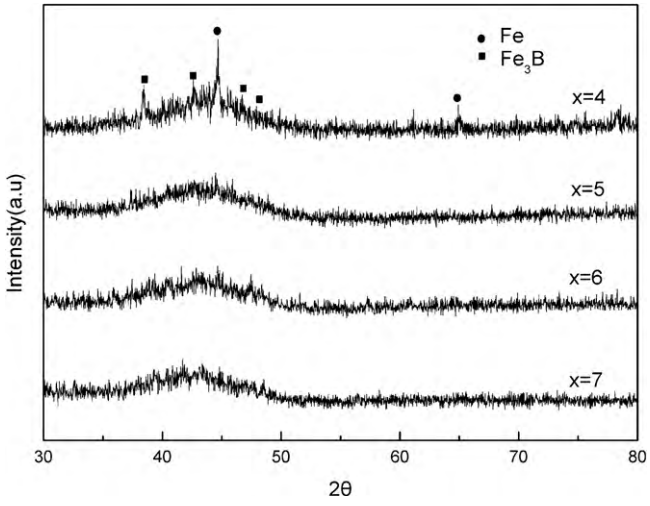

Fig. 1. XRD patterns of $(Fe_{72}Mo_4B_{24})_{100-x}Tb_x$ (x = 4, 5, 6, 7) alloy rods with diameter of 2 mm.

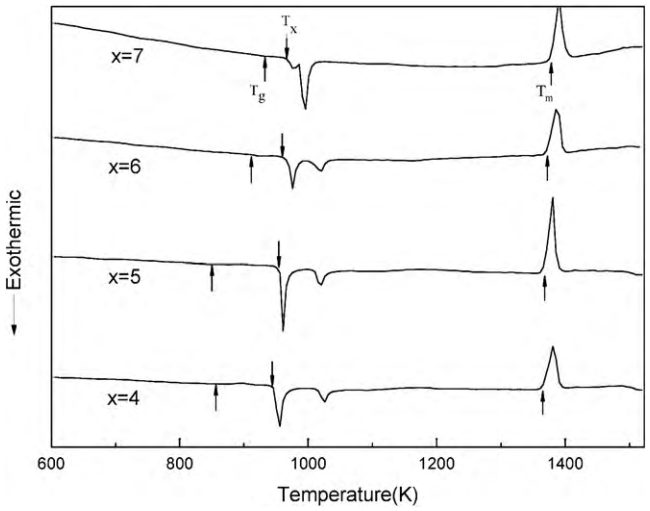

Fig. 3. DSC curves for $(Fe_{72}Mo_4B_{24})_{100-x}Tb_x$ (x = 4, 5, 6, 7) alloys.

operated at 300 keV was also employed to characterize the microstructure. Thermal stability was studied by differential scanning calorimeter (DSC) at a heating rate of 20 K/min. Mechanical properties, including compression strength and Young's modulus, were measured with a mechanical testing machine. The gauge dimension was 2 mm in diameter and 4 mm in length and the strain rate was $5 \times 10^{-4}\ s^{-1}$. Vickers hardness (H_v) was measured with a hardness tester under a load of 1.96 N. Magnetic properties of the alloy rods were measured by a vibrating sample magnetometer (VSM). The Curie temperature (T_c) was determined by a thermal gravimetric analyzer (TGA) with an externally applied magnetic field.

3. Results and discussion

Fig. 1 shows XRD patterns of $(Fe_{72}Mo_4B_{24})_{100-x}Tb_x$ (x = 4, 5, 6, 7) alloy rods with a diameter of 2 mm. There are some crystalline peaks on the basis of broad peak for x = 4, which could be identified as Fe and Fe_3B phases, respectively. The small intensity of diffraction peaks indicates that grain sizes of the crystalline phases were in nano-scales. Further increasing Tb content to x = 5, 6, and 7, XRD patterns show only broad peaks, indicating single amorphous structure in these alloys. It is therefore concluded that bulk amorphous alloy rods with diameter of 2 mm are obtained in $(Fe_{72}Mo_4B_{24})_{100-x}Tb_x$ (x = 5, 6, 7).

To confirm the crystalline phases in $(Fe_{72}Mo_4B_{24})_{96}Tb_4$, high-resolution TEM micrograph and the corresponding selected area diffraction (SAD) pattern are shown in Fig. 2. It can be seen that crystalline particles formed among the amorphous matrix, and the size of these crystalline particles was <200 nm in Fig. 2(a). The SAD pattern showed clear diffraction dots of crystalline phases based on the halo diffuse ring of the amorphous matrix. Meanwhile, crystalline particles were only found at the center region of the disk sample, where the cooling rate was relatively lower than that of the margins. From the calculated lattice distances by the SAD pattern in Fig. 2(a) and the XRD pattern in Fig. 1, it can be confirmed that α-Fe and Fe_3B existed simultaneously in the particles with small lattice deformation.

DSC was performed to investigate the thermal stability of $(Fe_{72}Mo_4B_{24})_{100-x}Tb_x$ system. Fig. 3 shows the DSC curves of $(Fe_{72}Mo_4B_{24})_{100-x}Tb_x$ (x = 4, 5, 6, 7) amorphous alloys. For $(Fe_{72}Mo_4B_{24})_{96}Tb_4$, the DSC curve represents structure evolution of the remaining amorphous matrix during heating process. The amorphous alloys exhibited distinct glass transition and supercooled liquid region. Glass transition temperature (T_g), crystallization temperature (T_x), supercooled liquid region ΔT_x ($=T_x - T_g$), melting temperature (T_m) as well as temperature of crys-

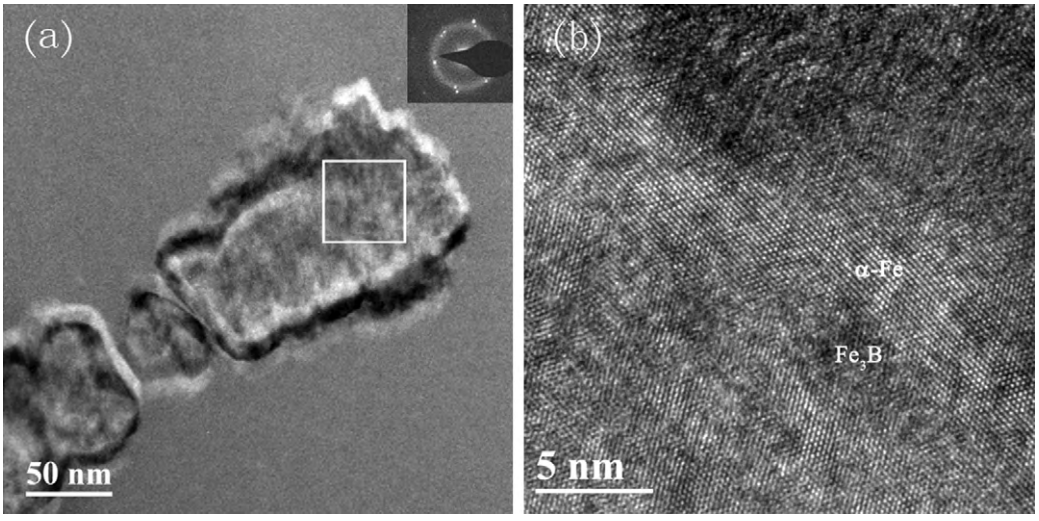

Fig. 2. (a) TEM micrograph of $(Fe_{72}Mo_4B_{24})_{96}Tb_4$ alloy; the inset at the upper right corner shows selected area diffraction pattern. (b) High-resolution TEM of the selected area in (a).

Table 1
Thermal parameters for $(Fe_{72}Mo_4B_{24})_{100-x}Tb_x$ (x = 4, 5, 6, 7) alloys.

$(Fe_{72}Mo_4B_{24})_{100-x}Tb_x$	T_g (K)	T_x (K)	ΔT_x (K)	T_{peak1} (K)	T_{peak2} (K)	T_m (K)
x = 4	856.0	944.0	87.9	952.1	1024.1	1365.0
x = 5	847.9	952.0	104.1	959.8	1018.7	1368.0
x = 6	911.2	960.0	48.4	973.9	1018.8	1372.0
x = 7	927.0	966.3	39.3	977.3	992.3	1378.3

tallization peaks (T_{peak1}, T_{peak2}) for $(Fe_{72}Mo_4B_{24})_{100-x}Tb_x$ (x = 5, 6, 7) and amorphous matrix of $(Fe_{72}Mo_4B_{24})_{96}Tb_4$ are listed in Table 1. This alloy system exhibited high glass transition temperatures (T_g > 800 K), which was higher than the Fe–Nb–B–Y system [22]. T_g first decreased from 856.0 K to 847.9 K as Tb content increased from 4% to 5%, then went up to 927.0 K as Tb content increased to 7%, while T_x continuously increased from 944.0 K to 966.3 K. As Tb content increased, ΔT_x (=$T_x - T_g$) first increased from 87.9 K to 104.1 K, then decreased to 39.3 K. The largest supercooled liquid region of 104.1 K was obtained in $(Fe_{72}Mo_4B_{24})_{95}Tb_5$. Its supercooled liquid region was also wider than that of Fe–Nb–B–Y system, which was limited to 50 K [22]. Both the high glass transition temperature and wide supercooled liquid region indicate that this alloy system has very good thermal stability.

In Fe-based BMG systems, supercooled liquid region ΔT_x is often used to measure the glass forming ability. Thus, the largest supercooled liquid region of $(Fe_{72}Mo_4B_{24})_{95}Tb_5$ indicates that this alloy has the best glass forming ability. As can be seen in the DSC curves, the temperature interval between two crystallization peaks gradually decreased with the increase of Tb content, and the intensity ratio of first crystallization peak to second crystallization peak was the largest in $(Fe_{72}Mo_4B_{24})_{95}Tb_5$. It had been pointed out that the intensity of the first crystallization peak partially indicated the difficulty of crystallization, which furthermore indicated stability of supercooled liquid region [29]. Thus, the best glass forming ability of $(Fe_{72}Mo_4B_{24})_{95}Tb_5$ alloy is consistent with its strong intensity of first crystallization peak.

It has been demonstrated that the addition of Tb increased the glass forming ability of the alloy system. According to the turmoil principles [30], the more constituent elements of a system is, the higher its configuration entropy is, which leads to more stable liquid state, and therefore more difficult to crystallize. Secondly, the element radius of Tb is much larger than those of Fe, Mo, and B elements, and this is beneficial to amorphous structure in point of topology, leading to a dense random packing structure. Thirdly, negative mixing entropy between Tb–B is large, which is −51 kJ/mol [31]. Moreover, Tb has a purifying effect by absorbing oxygen to form Tb oxide and flow on the surface of molten alloy, leading to the suppression of heterogeneous nucleation and resulting in the improvement of the glass forming ability. Thus, good glass forming ability has been attained in the present alloy system.

Fig. 4 shows compressive curves of $(Fe_{72}Mo_4B_{24})_{100-x}Tb_x$ (x = 4, 5, 6, 7) amorphous rods. Mechanical parameters are listed in Table 2. Compressive curves show no ductility. Ultra-high compressive stress (σ_f) of 3951.6 MPa was obtained in $(Fe_{72}Mo_4B_{24})_{96}Tb_4$. As Tb content increased, where fully amorphous structure was obtained, compressive strength first decreased to 2220 MPa, then increased to 3163 MPa, while Young's modulus (E) first decreased

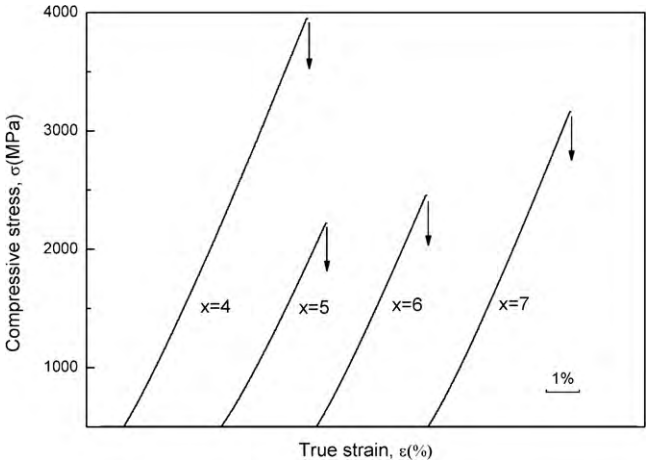

Fig. 4. Compressive true stress–strain curves of the $(Fe_{72}Mo_4B_{24})_{100-x}Tb_x$ (x = 4, 5, 6, 7) alloy rods.

from 60 GPa to 50 GPa, then increased to 61 GPa. In fully amorphous alloys, the highest compressive stress of 3163 MPa was obtained for x = 7 and this value was also higher than that of the best glass former $Fe_{74}Nb_6Y_3B_{17}$ in Fe–Nb–B–Y system [22]. However, compared with other similar Fe-based BMGs [32–33], this alloy system exhibited a relatively lower E and larger elastic strain up to 5%. H_v of the alloy system increased from 1118 to 1149 with the increase of Tb content.

$(Fe_{72}Mo_4B_{24})_{96}Tb_4$ exhibited the highest compressive stress. This can be explained by its special structure, which consists of nanocrystalline among amorphous matrix. In fully amorphous alloys, the high σ_f and H_v can be attributed to bonding nature of constituent elements. It has been pointed out by Chen et al. [34] that electrons could transfer from the metalloid elements to fill the d shells of transition mental elements, and then s-d hybrid bonding is formed. In this alloy system, Mo holds one 5s electron, while B holds two 2s electrons. It is considered that one 5s electron of Mo is more active than the two 2s electrons of B, because the energy level of a pair of s electrons with inverse spin direction is much lower than that of one s electron. Therefore, the 5s electron from Mo would transfer more easily than those from B, leading to strong s-d hybrid bonding nature. Moreover, the large mixing entropy of −51 kJ/mol between Tb and B is also beneficial to a very strong bonding strength [35]. So the alloy system exhibits large compressive strength and hardness (H_v), and both σ_f and H_v increase with increase of Tb content.

Table 2
Magnetic and mechanical parameters for $(Fe_{72}Mo_4B_{24})_{100-x}Tb_x$ (x = 4, 5, 6, 7) alloys.

$(Fe_{72}Mo_4B_{24})_{100-x}Tb_x$	M_s (emu/g)	H_c (Oe)	λ_s (ppm)	T_c (K)	σ_f (MPa)	H_v	E (GPa)
x = 4	78.231	4.289	19	480.46	3951.6	1118.43	60
x = 5	69.205	19.131	21	459.33	2220.2	1118.46	57
x = 6	56.327	26.077	18	455.61	2455.5	1125.90	50
x = 7	52.211	4.639	11	439.18	3163.8	1149.78	61

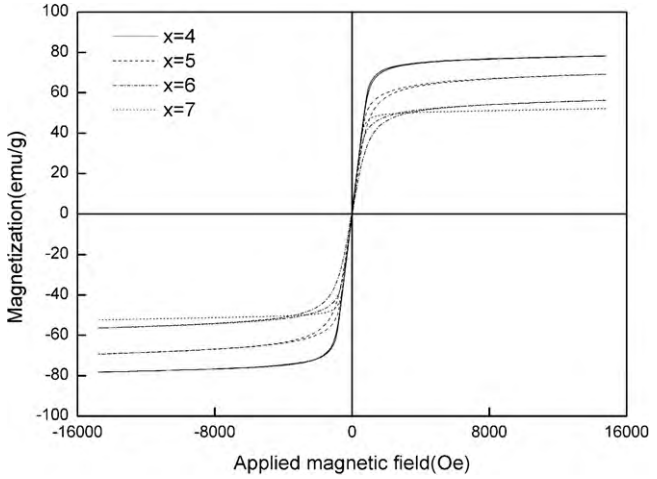

Fig. 5. Magnetization hysteresis loops of as-cast $(Fe_{72}Mo_4B_{24})_{100-x}Tb_x$ (x = 4, 5, 6, 7) alloys measured at room temperature.

Fig. 5 represents hysteresis loops of $(Fe_{72}Mo_4B_{24})_{100-x}Tb_x$ (x = 4, 5, 6, 7) amorphous rods. Magnetic parameters, including saturation magnetization (M_s), coercivity (H_c), saturation magnetostriction (λ_s), Curie temperature (T_c), are listed in Table 2. It can be seen in Fig. 5 that magnetization quickly saturated under the applied magnetic field, indicating soft magnetic properties in this alloy system. $(Fe_{72}Mo_4B_{24})_{96}Tb_4$ exhibited the best soft magnetic property, with M_s of 78.231 emu/g, H_c of 4.289 Oe and T_c of 480.46 K. As Tb content increased from 5% to 7%, M_s decreased from 69.205 emu/g to 52.211 emu/g monotonously, whereas, H_c first increased from 19.131 Oe to 26.077 Oe, then decreased to 4.639 Oe, and T_c decreased from 459.33 K to 439.18 K monotonously.

In Fe-based amorphous alloys, ferromagnetism derives mainly from the Fe moment. With the increase of Tb content, Fe content decreases, therefore saturation magnetization decreases. Curie temperature is a measurement of the intensity of exchange coupling between magnetic atomic moments. The exchange coupling between Fe atoms also decreases because of the dilution of Fe atoms, leading to the decrease of T_c. Coercivity of the present alloys might be affected by the internal stress, which needs to be further investigated. As to $(Fe_{72}Mo_4B_{24})_{96}Tb_4$, both its special structure and high Fe content lead to good soft magnetic property.

4. Conclusions

BMG alloy system $(Fe_{72}Mo_4B_{24})_{100-x}Tb_x$ (x = 4, 5, 6, 7) has been explored in this work. Main conclusions are drawn as follows:

(1) Amorphous rods with diameter of 2 mm were prepared in $(Fe_{72}Mo_4B_{24})_{100-x}Tb_x$ (x = 5, 6, 7). Fully amorphous $(Fe_{72}Mo_4B_{24})_{95}Tb_5$ has the best glass forming ability and a large supercooled liquid region up to 104 K. Good soft magnetic properties are also obtained when x = 5, with M_s up to 69.205 emu/g. In addition, this amorphous alloy system possesses good mechanical properties, with σ_f of 2220–3163 MPa and H_v up to 1149.

(2) In $(Fe_{72}Mo_4B_{24})_{96}Tb_4$, nanocrystalline Fe_3B and α-Fe were precipitated at the amorphous matrix, exhibiting enhanced mechanical properties with σ_f of 3951 MPa and much better soft magnetic properties with M_s of 78.231 emu/g and H_c of 4.289 Oe, respectively.

Acknowledgements

This work was supported by National Natural Science Foundation of China (NSFC 50971113), Visiting Scholar Foundation of State Key Laboratory of Silicon Materials (SKL2009-6) and the Program for Changjiang Scholars and Innovative Research Team in University (PCSIRT-0651).

References

[1] A. Inoue, Y. Shinohara, J.S. Gook, Mater. Trans. JIM 36 (1995) 1427.
[2] A. Inoue, Mater. Trans. JIM 36 (1995) 866.
[3] B.L. Shen, H. Kimura, A. Inoue, T. Mizushima, Mater. Trans. 42 (2001) 660.
[4] A. Makino, C. Chang, T. Kubota, A. Inoue, J. Alloys Compd. 483 (2009) 616.
[5] A. Inoue, Z. Tao, A. Takeuchi, Appl. Phys. Lett. 71 (1997) 464.
[6] P. Pawlik, H.A. Davies, M.R.J. Gibbs, Appl. Phys. Lett. 83 (2003) 2275.
[7] P. Pawlik, H.A. Davies, J. Non-Cryst. Solids 329 (2003) 17.
[8] D.Y. Liu, W.S. Sun, A.M. Wang, H.F. Zhang, Z.Q. Hu, J. Alloys Compd. 370 (2004) 249.
[9] C.Y. Lin, H.Y. Tien, T.S. Chin, Appl. Phys. Lett. 86 (2005) 162501.
[10] J.H. Yao, J.Q. Wang, Y. Li, Appl. Phys. Lett. 92 (2008) 251906.
[11] I. Betancourt, R. Landa, J. Alloys Compd. 481 (2009) 87.
[12] S.F. Guo, Z.Y. Wu, L. Liu, J. Alloys Compd. 468 (2009) 54.
[13] M. Stoica, S. Kumar, S. Roth, S. Ram, J. Eckert, G. Vaughan, A.R. Yavari, J. Alloys Compd. 483 (2009) 632.
[14] B.L. Shen, A. Inoue, Appl. Phys. Lett. 85 (2004) 4911.
[15] T. Bitoh, A. Makino, A. Inoue, J. Appl. Phys. 99 (2006), 08F102.
[16] A. Inoue, B.L. Shen, C.T. Chang, Acta Mater. 52 (2004) 4093.
[17] C. Duhamel, K.G. Georgarakis, A. LeMoulec, A.R. Yavari, G. Vaughan, A. Baron, N. Lupu, J. Alloys Compd. 483 (2009) 243.
[18] A. Inoue, W. Zhang, J. Appl. Phys. 85 (1999) 4491.
[19] M. Imafuku, K. Yaoita, S. Sato, W. Zhang, A. Inoue, Y. Waseda, Mater. Sci. Eng. A-Struct. Mater. Prop. Microstruct. Process A304–306 (2001) 660.
[20] Y. Long, W. Zhang, X.M. Wang, A. Inoue, J. Appl. Phys. 91 (2002) 5227.
[21] X.M. Huang, X.D. Wang, Y. He, Q.P. Cao, J.Z. Jiang, Scr. Mater. 60 (2009) 152.
[22] D.S. Song, J.H. Kim, E. Fleury, W.T. Kim, D.H. Kim, J. Alloys Compd. 389 (2005) 159.
[23] H.W. Chang, Y.C. Huang, C.W. Chang, C.H. Chiu, W.C. Chang, J. Alloys Compd. 462 (2008) 68.
[24] S. Lee, H. Kato, T. Kubota, K. Yubuta, A. Makino, A. Inoue, Mater. Trans. 49 (2008) 506.
[25] H.W. Chang, Y.C. Huang, C.W. Chang, C.C. Hsieh, W.C. Chang, J. Alloys Compd. 472 (2009) 166.
[26] S.F. Guo, L. Liu, X. Lin, J. Alloys Compd. 478 (2009) 226.
[27] A. Inoue, B.L. Shen, H. Koshiba, H. Kato, A.R. Yavari, Nat. Mater. 2 (2003) 661.
[28] A. Hirata, Y. Hirotsu, K. Amiya, A. Inoue, Phys. Rev. B 78 (2008) 144205.
[29] B.L. Shen, C.T. Chang, T. Kubota, A. Inoue, J. Appl. Phys. 100 (2006) 013515.
[30] A.L. Greer, Nature 366 (1993) 303.
[31] A. Takeuchi, A. Inoue, Mater. Trans. 46 (2005) 2817.
[32] A. Inoue, B.L. Shen, Adv. Mater. 16 (2004) 2189.
[33] B.L. Shen, C.T. Chang, Z.F. Zhang, A. Inoue, J. Appl. Phys. 102 (2007) 023515.
[34] H.S. Chen, J.T. Krause, E. Coleman, J. Non-Cryst. Solids 18 (1975) 157.
[35] F.J. Liu, Q.W. Yang, S.J. Pang, T. Zhang, J. Non-Cryst. Solids 355 (2009) 1444.